SIMULATION OF GROWTH AND TRANSPORTATION OF SOLID INCLUSIONS IN INDUCTIONS FURNACES

M.Ščepanskis, A.Jakovičs (University of Latvia, Laboratory for Mathematical Modelling of Environmental and Technological Processes)
M.Brics (University of Rostock, Institute of Physics)
E.Baake, B.Nacke (W.G.Leibniz University of Hanover, Institute of Electrotechnology)

PREVIOUS INVESTIGATIONS, INDUSTRIAL APPLICATIONS AND PROBLEMS

The present paper deals with the transport of solid inclusions in a recirculated flow of metal melt in the metallurgical equipment – induction crucible and channel furnaces. All of them have the same physical principle of operation [1] and, consequently, the similar flow distribution in the active region. Alternating current in the inductor creates a magnetic field and induces alternating current in the conductive liquid metal. The result of the interaction of induced current and magnetic field is the Lorentz force, which drives the liquid away from the wall. As far as the vessel with liquid metal is closed and driving electromagnetic (EM) force has the maximum at the middle of the inductor, the flow consists of two main vortices in the cross section of the vessel: toroidal vortices in a cylindrical induction crucible furnace (ICF) [2], vortices in a channel of the induction channel furnace (CIF) [3]. However, the power of ICFs and CIFs is sufficiently high, enough to produce a turbulent flow with high Reynolds number (e.g. for laboratory ICF it is about 1E+5). Therefore the mentioned two vortices appear only in the time averaged case, but in practice at each moment the turbulent flow consists of numerous eddies with the different sizes, however the common structure of the flow remains quasistationary.

The flows in the induction furnaces are researched well numerically and experimentally. A.Umbrashko et. al compared the results of the experimental investigations of ICF and the Large Eddy Simulation (LES) results and conclude that only LES method allows to obtain the correct estimation of the turbulent parameters and can be used for solving fluid dynamics and thermal problems in practical melting applications [4]. The first measurements of the velocity field in the industrial scale CIF, which was filled with Wood's metal, were done by A.Eggers within his PhD work [5]. Later, when computational capacity increases, E.Baake et. al made LES simulations of the same CIF [6]. The last work verifies the averaged velocity field with the Eggers' experimental measurements and also made turbulent studies of the flow.

However, in spite of the fact that EM heating and stirring is one of the most effective and widespread methods for melting and processing of conductive materials, there are some essential industrial problems concerning the inclusion transport, and these processes are still poor investigated.

The alloying particles are mixed in a steel melt to improve properties like strength, hardness and wear resistance. It is important to achieve homogeneous admixtures distribution to ensure high quality of the alloy. Furthermore it is desirable to reduce the time of mixing to decrease the energy consumptions and prevent the melt from excessive overheating.

Unfortunately, there is no experimental technique (known by authors) that gives a possibility to study the dynamics of the particle motion inside the melt. The electric well-conductive materials are not optically transparent, but transparent liquids have low conductivity. D.R.Sadoway & J.Szekely tried to use transparent LiCl-KCl eutectic to reproduce the recirculation motion in an ICF [7], but they met with failure. EM field produces not only induced flow motion, but also heat up the liquid within the penetration depth. Thereby thermal convection dominates in the low-conductive transparent liquids. In spite of the optimistic conclusions of Sadoway & Szekely, the non-published simulation, which is done by the authors of the present paper, shows that it is not possible to avoid the thermal motion by changing the EM conditions. Therefore this liquid cannot be used to produce such flow patterns. The only known more or less successful method, developed in S.Taniguchi's group (see e.g. [8]), gives the possibility to investigate experimentally the rate of the particle

deposition in a turbulent flow of liquid metal under EM force. However, because the results are obtained by cutting solidified liquid, it is impossible to receive any information about the dynamics of the process inside the melt using such experimental technique. Moreover, the presence of the solidification front has an influence on the particles during the solidification and it is not clear, if this effect is negligible.

Because of the absence of the relevant experimental technique, the numerical simulation becomes the only possibility to estimate the optimal conditions of the admixing of inclusions (such as the size of alloying particles, the time of the mixing, geometry of device and other parameters). So M.Ščepanskis et. al simulated the dynamics of the homogenization of alloying particles in the ICF of the laboratory scale [9]. This investigation lights the process dependence on the particle size and density.

The redistribution of the equal-sized small solid inclusions in CIF is also analyzed last years (see e.g. the recent paper [10]). However, the main problem concerning the CIF operation is the deposition of the impurities like oxides as well as the erosion of the walls of the channel. These processes can significantly reduce the efficiency of the equipment up to breakdown (channel clogging). As it is shown on the Figure 1, the rate of the clogging dramatically increases, when the impurities start to deposit in the porous substance, like a sponge. This regime of the fast clogging, which reduces the active cross section of the channel very fast, attracts the attention of the operators of furnaces. The authors believe that this sponge-like clogging can be fulfilled by the depositing big particles, which previously grew in the bulk of the melt. Taking into account this hypothesis, it becomes clear that the simulation of the particles with invariable size is not completely relevant to the porous clogging problem and the size evolution of inclusions should be taken into account. The present paper, unfortunately, does not give the full answer for this problem, but contains the estimations of the size changing rate of the particles while the CIF is operated.

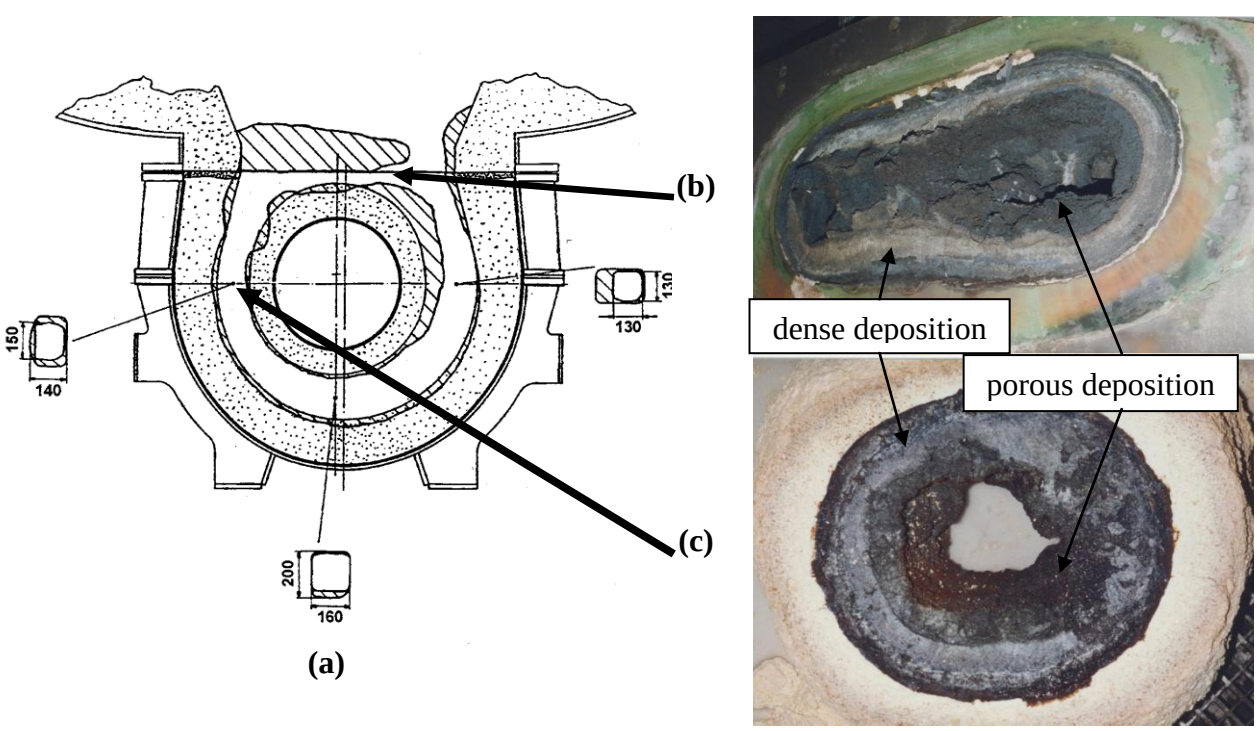

Figure 1. (a) - the scheme of the build-up formations in the channel of 1200 kW cast-iron-inductor CIF after a 14 month long operation [11]. (b) and (c) – the photos of clogged cross-sections of the neck and the channel of the CIF respectively (courtesy ABB Dortmund).

TRANSPORTATION OF INCLUSIONS

The present transport model includes the simulation of the flow and the particle motion. The flow is driven by EM force and thermal buoyancy force in the Boussinesq approximation. As in [2], [4] and [9], the turbulence is calculated using the LES method with the isotropic Smagorinsky subgrid viscosity model. The solid inclusions are calculated adopting the LES-based Euler-Lagrange approach in the limit of dilute conditions (one-way coupling). This assumption is possible because the volume of the inclusions does not exceed 1-2% of the liquid volume. The rigid spheres are also assumed. The Lagrange equation describes the motion of the inertia non-conductive spherical particles [12]:

$$\underbrace{\left(1+\frac{C_A}{2}\frac{\rho_f}{\rho_p}\right)\cdot\frac{d\mathbf{u}_p}{dt}}_{d\mathbf{u}_p/dt+added\,mass\,force}=\underbrace{C_D\cdot\mathbf{U}}_{drag\,force}+\underbrace{\left(1-\frac{\rho_f}{\rho_p}\right)\cdot\mathbf{g}}_{buoyancy\,force}-\underbrace{\frac{3}{4}\frac{1}{\rho_p}\mathbf{f}_{em}}_{EM\,force}+\underbrace{\frac{\rho_f}{\rho_p}C_L\boldsymbol{\xi}}_{lift\,force}+\underbrace{\left(1+\frac{C_A}{2}\frac{\rho_f}{\rho_p}\right)\cdot\frac{D\mathbf{u}_f}{Dt}}_{acceleration+added\,mass}, \qquad (1)$$

where $\boldsymbol{U}=\boldsymbol{u}_f-\boldsymbol{u}_p$, $\boldsymbol{u}_f$ and $\boldsymbol{u}_p$ are liquid and particle velocities respectively, ρ_f and ρ_p are liquid and particle density respectively, $\boldsymbol{g}$ is free fall acceleration; $\boldsymbol{f}_{em}=0.5\cdot(\boldsymbol{j}\times\boldsymbol{B}^*)$ is the averaged Lorenz force density, $\boldsymbol{j}$ is current density, $\boldsymbol{B}^*$ is complex conjugated magnetic field induction, $\boldsymbol{\xi}=\boldsymbol{U}\times(\nabla\times\boldsymbol{U})$; $C_A(dU/dt,U)$, $C_D(U)$ and $C_L(U)$ are acceleration, drag and lift force coefficients respectively.

It is statistically proved that the used Lagrange equation (1) for particle tracking in ICF should include drag, EM, buoyancy, lift, acceleration and added mass forces [12]. The relevant approximations for the forces are chosen on the basis of the statistical analysis of the non-dimensional parameters (particle Reynolds number, shear stress and acceleration parameter).

It should be also mentioned that we know only the filtered velocity in the LES framework and assume the isotropy of the subgrid part. In spite of the calculation of the individual trajectories of particles, the analysis will be done for the cloud, so the unfiltered isotropic part of velocity should not significantly influence the common results.

As far as the hydrodynamics is simulated using open source *OpenFOAM* software, the coupled Lagrange block is also coded within the same software. The particle tracking library is supplemented with EM, lift, acceleration and added mass forces. Thereby the Lagrange equation becomes non-linear. To ensure the convergence the hydrodynamic time step was split into various Lagrange time steps (LTS). The non-linear factors in the Lagrange equation are approximated with the values that correspond to the previous LTS (the Pikar's method). The implicit scheme is used to solve the equation. Moreover the *OpenFOAM* algorithm does not take into account the collision of a particle with the wall in a situation when the size of the particle is larger than the size of a mesh element. If the distance between the particle center and the wall is smaller than the radius, than the present model moves the particle to the distance of the radius from the wall at the end of the each LTS.

Let us present now some results concerning the particle transport in ICF, these results were obtained using the model described above. The first row of Figure 2 represents the snapshots of the carbon admixing in the ICF, which is one of the typical steel making step, operated in cylindrical furnaces. As far as liquid metal is not transparent, industrial observations is possible only on the top surface of the melt. We can see from the photos that some of the particles join the slag, which is usually situated in the corner between the wall and the free surface of the crucible. The numerical model does not take into account the presence of the slag, but however the results of the simulation (second row of Figure 2) can satisfactorily represent the industrial photo in the first row. The last row of Figure 2 shows in addition the motion of the carbon particle in the bulk of liquid metal (simulated), which is invisible. This motion can be also observed on Video 1 (see appendix). 57 cm high and 33.6 cm wide ICF is simulated here, the typical velocity of the flow is 15 cm/s.

After the initial period, which is shown on Figure 2, the inclusions become distributed mainly in the zones of the eddies. Then the distribution of the particles become even due to the exchange of the particles between the main eddies through the unstable middle zone [9]. Hydrodynamic

instabilities disturb the regular EM induced flow structure with two toroidal eddies and produce large axial pulsations in the middle zone near the wall, which were investigated experimentally and numerically [2], [4]. These pulsations result in the oscillating nature of the particle exchange and, consequently, the homogenization process [13].

The behavior of the cloud of equal-sized particles in CIF is analyzed as well within the research group of the present authors and also published in the proceeding of this conference [14]. That paper deals with the smallest particles, therefore the inertia forces, except drag, buoyancy and EM forces, are neglected. This assumption allows to use the commercial software *FLUENT* for the hydrodynamics and the particle calculation. However, it should be underlined that this simplified model is not relevant for the bigger particles, which are of interest concerning the sponge-like clogging of the channel. Nevertheless, the analysis in [14] shows that the particles can slowly migrate along the channel, come to the bath from the channel and vice versa. The further investigation will be focused on the changes of the particle size in the channel and the bath of CIF.

Before the next chapter, where the particle growth will be estimated, the increase of the significance of EM force, and, consequently, the deposition rate, with the increase of particle sizes should be emphasized. This phenomenon is illustrated and theoretically explained in [9]. Therefore the analysis of the growth of the inclusions in the bulk of the melt is important for the investigation of the deposition processes.

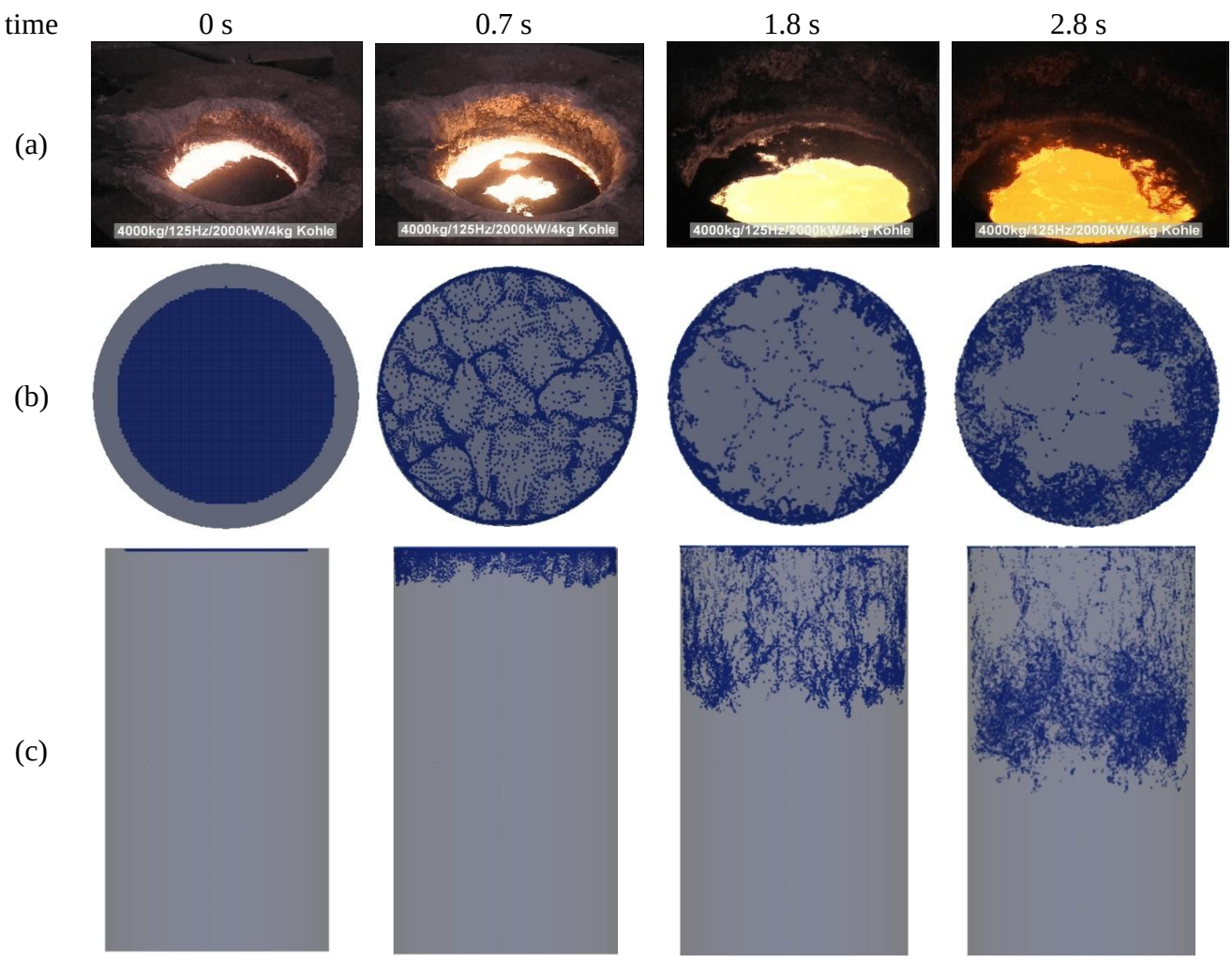

Figure 2. Carbon admixing into the steel alloy in ICF. (a) – snapshots of industrial process (courtesy Otto Junker GmbH), (b) - simulated results, view on the top of the furnace, (c) – particles in the bulk of the flow, view from side. Simulated particles are 100 μm in diameter and liquid-to-particle density ratio $S = \rho_f / \rho_p = 1.5$.

GROWTH OF THE INCLUSIONS

The process of the size evolution of inclusions can be provided by two different physical phenomena:

- diffusion limited Ostwald ripening [15],
- collisions of the particles and clustering.

Ostwald ripening is the process of dissolution of small particles and the redeposition of the dissolved material on the surfaces of larger particles. This thermodynamically-driven spontaneous process occurs because larger particles are more energetically favoured than smaller particles. The system tries to lower its overall energy, so molecules on the surface of a small particle will diffuse into the solution. When all small particles do this, the free atoms in solution are supersaturated and condense on the surface of larger particles. Therefore, all smaller particles shrink, while larger particles grow, and overall the average size will increase. After an infinite amount of time, the entire population of particles will have become one, huge, spherical particle to minimize the total surface area. But due to EM force this asymptotical state will be not achieved and the particles with arbitrary size will be removed from the melt by deposition on the wall.

Lifshitz & Slyozov performed a mathematical investigation of Ostwald ripening [16]. Steady-state concentration C_{R} (volume concentration) close to the surface of a particle depends on the radius R as follows:

$$C_{\mathrm{R}} = C_{\infty} + \frac{\alpha}{R}, \qquad \alpha = \frac{\sigma}{\mathrm{k}T}\mathrm{V_a}\, C_{\infty},$$

where C_{∞} is the concentration of saturated solution, σ is surface tension, k =1.38E-23 J/K is Boltzmann constant, T is temperature, $\mathrm{V_a}$ is the volume of the atom of dissolved substance.

Assuming supersaturation rate $\Delta = C - C_{\infty} << 1$ (C is particular volume concentration of impurities), we can express the diffusion flow of the dissolved substance per area unit as follows:

$$j = D\left.\frac{\partial C}{\partial r}\right|_{r=R} = \frac{D}{R}(C - C_{\mathrm{R}}) = \frac{D}{R}\left(\Delta - \frac{\alpha}{R}\right), \tag{2}$$

where D is diffusion coefficient. Consequently

$$\frac{\mathrm{d}R}{\mathrm{d}t} = \frac{D}{R}\left(\Delta - \frac{\alpha}{R}\right). \tag{3}$$

When the radius of the particle is equal to its critical value $R_{\mathrm{cr}} = \alpha/\Delta$ (the solution of the stationary equation), the particle is in the tranquility with the solution. If $R > R_{\mathrm{cr}}$, the particle grows, otherwise dissolves. We should underline that Δ and consequently R_{cr} changes in time as the function of temperature and concentration. However, the changes of the particle size should be calculated within each step of time, which is used for the calculation of hydrodynamics, temperature and concentration fields. Thereby, assuming $R(t=0) = \mathrm{R}_0$, we can obtain the solution of differential equation (2) for instant Δ and $\mathrm{R_{cr}}$:

$$t \cdot \mathrm{D}\Delta = \frac{R^2 - \mathrm{R}_0^2}{2} + \mathrm{R_{cr}} \cdot (R - \mathrm{R}_0) + \mathrm{R_{cr}^2} \cdot \ln\frac{R - \mathrm{R_{cr}}}{\mathrm{R}_0 - \mathrm{R_{cr}}}$$

or the same in non-dimensional form:

$$t \cdot \vartheta = (r-1)\left(\frac{r+1}{2} + \mathrm{r_{cr}}\right) + \mathrm{r_{cr}^2} \cdot \ln\frac{r - \mathrm{r_{cr}}}{1 - \mathrm{r_{cr}}}, \tag{4}$$

where $r = R/\mathrm{R}_0$, $\mathrm{r_{cr}} = \mathrm{R_{cr}}/\mathrm{R}_0$ and $\vartheta = \mathrm{D}\Delta/\mathrm{R}_0^2$. Figure 3 shows the solution of equation (4). Only $\mathrm{r} < 1$ solution is meaningful, if $\mathrm{r_{cr}} > 1$, and only $\mathrm{r} > 1$ otherwise. This means that the particle, which is larger than critical one, will grow and dissolve otherwise. As far as $f(r)$, which stands for the right part of equation (4), is monotonous, the Newton method can be used to solve the equation $f(r) - \vartheta t = 0$.

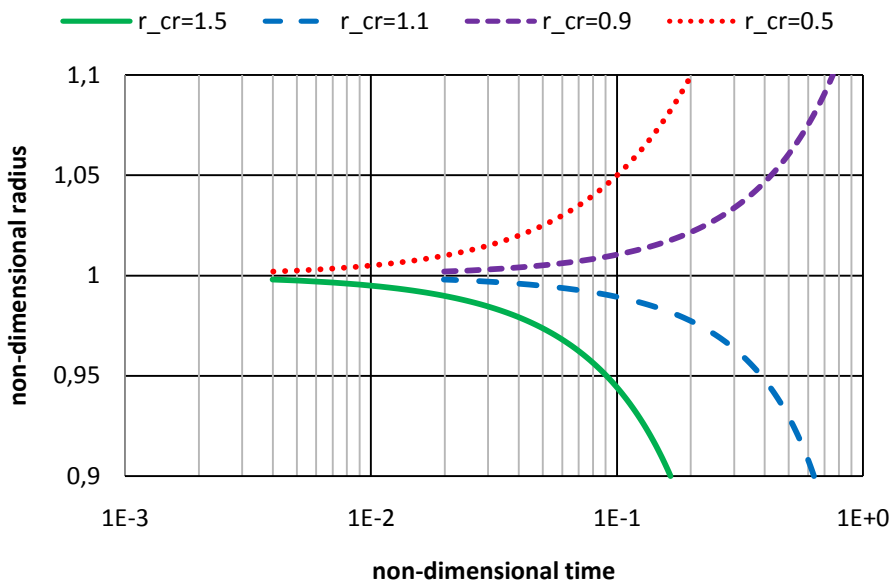

Figure 3. The diffusion limited growth / dissolution of a particle, assuming instant supersaturation rate Δ and the critical radius R_{cr}. Non-dimensional radius r depending on non-dimensional time $(t \cdot \vartheta)$ for different non-dimensional critical radius r_{cr}.

For the particular inclusions $R_{cr} = \alpha/\Delta = (\sigma V_a C_\infty)/(kT\Delta)$ and $\vartheta = D\Delta/R_0^2$ can be estimated through the expression for saturation concentration [17]

$$C_\infty(T) = \frac{\rho_{melt}}{\rho_{incl}}\left(1 + e^{\frac{\varepsilon}{RT}}\right)^{-1}, \quad (5)$$

where ρ_{melt} and ρ_{incl} are density of the melt and solid inclusions respectively, $R \cong 8.31$ J/(mol·K)$^{-1}$ and bounding energy ε can be calculated using thermodynamic expression [17]

$$\varepsilon = \varepsilon^{f}_{incl} + \varepsilon^{v}_{incl} - \sqrt{\varepsilon^{v}_{incl} \cdot \varepsilon^{v}_{melt}}, \quad (6)$$

where ε^{v}_{incl} and ε^{f}_{incl} are inclusion's enthalpy of vaporization and enthalpy of fusion respectively, ε^{v}_{melt} is metal's enthalpy of vaporization. Diffusion coefficient D can be find out following Stokes-Einstein estimation [18].

For the estimation of the significance of the particle collision we will follow the model, presented in [19]. As the equation of agglomeration phenomena, following relations are chosen by neglecting the term of velocity fluctuation which has a scarce contribution:

$$N^{T}_{ij} = 1.3\alpha_T\left(\frac{a_i + a_j}{2}\right)^3\sqrt{\frac{\rho_{melt} \cdot E}{\mu}} \cdot n_i n_j, \qquad \alpha_T = 0.727 \cdot \left[\frac{\mu_L}{A}\left(\frac{a_1}{2}\right)^3\sqrt{\frac{\rho_L E}{\mu_L}}\right]^{-0.242}, \quad (7)$$

$$N^{S}_{ij} = \frac{2\pi\Delta\rho g}{9\mu_L} \cdot (a_i + a_j)^3 \cdot \left|\frac{a_i - a_j}{2}\right| \cdot n_i n_j, \quad (8)$$

$$N^{B}_{ij} = \frac{2kT}{3\mu_L}\left(\frac{1}{a_i} + \frac{1}{a_j}\right)(a_i + a_j) \cdot n_i n_j, \quad (9)$$

$$N_{ij} = N^{T}_{ij} + N^{S}_{ij} + N^{B}_{ij}, \quad (10)$$

where N_{ij} represents the collision frequency per unit time and volume (the suffices T, S and B represent turbulent, Stokes and Brownian terms), $\Delta\rho$ is density difference between liquid steel and inclusions, a_i and a_j are diameters of inclusions, μ is dynamic viscosity of liquid metal, E is turbulent energy dissipation rate, n_i and n_j are number of inclusions per unit volume, $A = 0.45\text{E}{-}20$ J is Hamarker constant [20].

Let us estimate now the typical time of the growth / dissolution of the inclusions in the steel melt. We can assume aluminium oxide (Al_2O_3) as a typical inclusion. This material is usually about

65% of all inclusions in the steel melt in CIF [11]. Moreover, other less distributed inclusions, such as magnesium oxide (MgO) and silicon oxide (Si_2O), have close physical properties. Table 1 displays the time to double the particle volume (in the case of dissolution – decrease the volume 2 times), calculated according to the equations (4)-(10). The table shows that small particles (less than 0.1 μm) change their size mostly due to the Ostwald ripening process. Contrary, the turbulent collisions influence the growth of bigger particles. However, the typical time of the collision growth of big particles can be underestimated, because of probably overestimation of the concentration, which can result from the assumption of the equal concentration of each size group.

Table 1. Time to change twice the volume of a Al_2O_3 particle in a steel melt. Comparison of the collision and Ostwald ripening models. Presented results are calculated for 215 kW CIF, assuming the homogeny distributed inclusions with common volume concentration 1%, the concentration of the particles in each size group is assumed equal. The degree of turbulent energy dissipation rate ε is calculated equal to 1E-2 m^2/s^3.

The temperature of the melt is **100 K over the melting temperature** of steel

Diameter of particles, m	**Collision model** time, s	**Ostwald ripening**					
		Relative supersaturation Δ/C_∞					
		1E+0		1E-1		1E-2	
		process	time, s	process	time, s	process	time, s
1E-8	-	growth	2.82E-3	dissolution	6.45E-3	dissolution	4.50E-3
1E-7	1.42E+0	growth	2.18E-1	growth	2.82E+0	dissolution	6.45E+0
1E-6	2.00E+1	growth	2.13E+1	growth	2.18E+2	growth	2.82E+3
1E-5	2.03E+1	growth	2.13E+3	growth	2.13E+4	growth	2.18E+5
1E-4	2.03E+1	growth	2.13E+5	growth	2.13E+6	growth	2.13E+7

The temperature of the melt is **40 K over the melting temperature** of steel

Diameter of particles, m	**Collision model** time, s	**Ostwald ripening**					
		Relative supersaturation Δ/C_∞					
		1E+0		1E-1		1E-2	
		process	time, s	process	time, s	process	time, s
1E-8	-	growth	4.16E-3	dissolution	9.50E-3	dissolution	6.61E-3
1E-7	1.42E+0	growth	3.21E-1	growth	4.16E+0	dissolution	9.50E+0
1E-6	2.00E+1	growth	3.14E+1	growth	3.21E+2	growth	4.16E+3
1E-5	2.03E+1	growth	3.13E+3	growth	3.14E+4	growth	3.21E+5
1E-4	2.03E+1	growth	3.13E+5	growth	3.13E+6	growth	3.14E+7

Table 1 estimated the growth and dissolution of the particles for different values of the relative supersaturation. Let us estimate now this value at two scenario, which are favourable for the growth of the inclusions in CIF and, consequently, for the sponge-like build-up formation.

First scenario simulates the change of the temperature regime of the CIF operation. The power of the furnaces is decreased for weekends or night time, when the production is temporarily interrupted. Quickly changing the temperature of the melt, the supersaturation of the dissolved inclusions can appear as the difference between the saturated concentration at the temperatures of the working and weekend regimes. If we assume that the temperature is changed from 1883 K (100 K above the melting point of the steel) to 1823 K (40 K above the temperature of solidification), than we can calculate the relative supersaturation Δ/C_∞ =0.472. Table 2 shows the estimation of the time, which is necessary to double the volume of the particle according to this scenario. If we assume the weekend period about 2.2E+5 s, it becomes evident, that described processes can significantly increase the size of the inclusions and, consequently, favour the porous

clogging. Turbulent collisions will drive this process, if the concentration of big particles is enough, but at the opposite case the particles will growth also within Ostwald model. Moreover, due to the Ostwald ripening the smallest inclusions will rapidly achieve the size, when collision model gives significant results. Therefore the tracing of the inertia particles in CIF should be done, coupling it with the size evolution model. The authors plan to carry out this simulation soon.

Table 2. Time to change twice the volume of a Al_2O_3 particle in a steel melt, assuming the relative supersaturation 0.472, which corresponds approximately to the transitions from working to weekend regime of the CIF operation. The other parameters are the same as in the Table 1.

Diameter of particles,	**Collision model**	**Ostwald ripening**	
m	time, s	process	time, s
1E-7	1.42E+0	growth	6.99E-1
1E-6	2.00E+1	growth	6.66E+1
1E-5	2.03E+1	growth	6.31E+3
1E-4	2.03E+1	growth	6.28E+5

Second scenario describes the growth of particle, travelling along the channel of CIF. E.Baake et. al simulated the temperature distribution in CIF [3] and found the melt in the channel overheated for at least 34 K in respect to the melt temperature in the bath. Taking into account the low velocity of the transit flow in the channel, the time, when the particle migrates along the channel, can be estimated as 1 min [10]. Assuming the linear distribution of the temperature along the channel (from the maximum in the lowest point and the minimum at the neck) and using equations (3) and (5), we can estimate the growth of the particle – the results are shown on Table 3. The growth of the particles according to this scenario is not so significant as it is at the first scenario, however, the coupling of them can give more precise results of the neck clogging.

Table 3. The estimation of the increase of the particle after the travel through the channel of CIF. The channel overheat is assumed linearly distributed from the neck to the maximum of 34 K over the neck temperature at the lower point of the channel. The time of the particle travel is assumed equal to 1 min.

Initial radius of the particle R_0, m	Relative increase of the particle R/R_0 -1
1E-7	3.7E+0
1E-6	1.1E-1
1E-5	1.2E-3
1E-4	1.2E-5
1E-3	1.2E-7

CONCLUSIONS

It is industrially observed, that the dangerous fast clogging of the channel in CIF is associated with sponge-like (porous) build-up formation. The authors put forward the hypothesis, that this porous clogging is fulfilled by deposition of the big inclusion, which previously grow in the bulk of the melt. For this reason the process of particle transportation and growth is analyzed.

The theoretical investigation stressed two possible physical phenomena, which can lead to the growth of the inclusions:

- diffusion limited Ostwald ripening;
- turbulent collisions and clustering.

For more convenient analysis the non-dimensional solution of Lifshitz & Slyozov mathematical model for Ostwald ripening of the single grain is obtained within this work. This solution is limited with the assumption of the quasi-instant parameters: diffusion coefficient, supersaturation and saturation concentration are invariable during the time of solution.

At last, the estimations of the inclusion growth time affirm the significance of the size evolution model for the prediction of the deposition rate. The smallest particles will rapidly dissolve under the Ostwald ripening process. But bigger inclusion will growth due to both mentioned physical phenomena. If the concentration of the inclusions of big diameter will be enough, the turbulent collisions will mostly drive the changes of the distribution of inclusion size. The Ostwald ripening will have greater role otherwise.

The estimations show that the average size of the inclusions can significantly increase during the weekend, when the furnace is switched to the lower power regime. This process can ensure the sponge-like clogging. Moreover, travelling along the channel small particles also rapidly increase their size and shift the maximum of the size distribution even greater.

The present estimations confirm the necessity of the particle tracking simulation in CIF, coupled with the size evolution model. These simulations will be done soon by the authors.

ACKNOWLEDGEMENTS

The contribution of M.Ščepanskis to the present work has been partly supported by the European Social Fund within the project „Support for Doctoral Studies at University of Latvia".

M.Brics contributes the paper during the ERASMUS internship at University of Latvia, the author thanks DAAD (German Academic Exchange Service) for this opportunity.

REFERENCES

[1] E.DÖTSCH *Inductive melting and holding* Essen: Vulkan-Verlag 2009

[2] M.KIRPO, A.JAKOVIČS, E.BAAKE and B.NACKE Analysis of experimental and simulation data for the liquid metal flow in a cylindrical vessel *Magnetohydrodynamics* **43** (2007) 161-72

[3] E.BAAKE, A.JAKOVIČS, S.PAVLOVS and M.KIRPO Long-term computations of turbulent flow and temperature field in the induction channel furnace with various channel design *Magnetohydrodynamics* **46** (2010) 461-74

[4] A.UMBRASHKO, E.BAAKE, B.NACKE and A.JAKOVIČS Modeling of the turbulent flow in induction furnaces *Metall. Mater. Trans. B* **37B** (2006) 831-8

[5] A.EGGERS *Untersuchungen der Schmelzenströmung und des Wärmetransports im Induktions-Rinnenofen* Fortschr.-Ber. VDI Reihe 19 Nr. 63 Düsseldorf: VDI-Verlag 1993 (in German)

[6] E.BAAKE, M.LANGEJUERGEN, M.KIRPO and A.JAKOVIČS Analysis of transient heat and mass transfer processes in the melt of induction channel furnaces using LES *Magnetohydrodynamics* **45** (2009) 385-91

[7] D.R.SADOWAY and J.SZEKELY A new experimental technique for the study of turbulent electromagnetically driven flows *Metall. Trans. B* **11B** (1980) 334-6

[8] S.TANIGUCHI and J.K.BRIMACOMBE Application of pinch force to the separation of inclusion particles from liquid steel *ISIJ International* **34** (1994) 722-31

[9] M.ŠČEPANSKIS, A.JAKOVIČS and B.NACKE Homogenization of non-conductive particles in EM induced metal flow in a cylindrical vessel *Magnetohydrodynamics* **46** (2010) 413-23

[10] S.PAVLOVS, A.JAKOVIČS, E.BAAKE, B.NACKE and M.KIRPO LES modelling of turbulent flows, heat exchange and particle transport in industrial induction channel furnaces *Magnetohydrodynamics* **47** (2011) 399-412

[11] R.DREWEK *Verschleißmechanismen in Induktions-Rinnenöfen für Gußeisen und Aluminium* Forschr.-Ber. VDI Reihe 21 Nr. 193 Düsseldorf: VDI-Verlag 1996 (in German)

[12] M.ŠČEPANSKIS, A.JAKOVIČS and E.BAAKE Statistical analysis of the influence of forces on particles in EM driven recirculated turbulent flows *J. Phys.: Conf. Ser.* **333** (2011) 012015

[13] M.ŠČEPANSKIS, A.JAKOVIČS, E.BAAKE and B.NACKE The oscillations appearing during the process of particle homogenization in EM induced flow of ICF *Proc. 8th Int. Pamir Conf. on Fundamental and Applied MHD* Borgo (Corsica, France) 2011 **2** 653-7

[14] S.PAVLOVS, A.JAKOVIČS, E.BAAKE and B.NACKE LES long-term analysis of particles transport in melt turbulent flow for industrial induction channel furnaces *Proc. 8th Int. Conf. on Clean Steel* Budapest (Hungary) 2012

[15] L.RATKE and P.W.VOORHEES *Growth and coarsening: Ostwald ripening in material processing* Berlin, Heidelberg, New York, Barcelona, Hong Kong, London, Milan, Paris, Toyo: Springer 2002
[16] I.M.LIFSHITZ and V.V.SLYOZOV The kinetics of precipitation from supersaturated solid solution *J. Phys. Chem. Sol.* **19** (1961) 35-50
[17] U.BETHERS, A.JAKOVICS, N.JEKABSONS, I.MADZULIS and B.NACKE Theoretical investigation of the conditions of the build-up formation in induction channel furnaces *Magnetohydrodynamics* **30** (1994) 201-210
[18] A.EINSTEIN. Eine neue Bestimmung der Molekuldimensionen *Analen der Physic* **19** (1906) 289-305 (in German)
[19] T.TOH, H.YAMAMURA, H.KONDO, M.WAKOH, S.SHIMASAKI and S.TANIGUCHI Kinetic evaluation of inclusions removal during levitation melting of steel in cold crucible *ISIJ Internationa* **47** (2007) 1625-32.
[20] S.TANIGUCHI and A.KIKUCHI Removal of non-metallic inclusion from liquid metal by AC-electromagnetic force *Proc. 3rd Symp. on Electromagnetic Processing of Materials* Tokyo (Japan) 2000 315-20